Atomic H-Induced Mo₂C Hybrid as an Active and Stable Bifunctional Electrocatalyst—Supporting Information

Xiujun Fan,[†‡⊥∥] * Yuanyue Liu,[¶ς] Zhiwei Peng,[⊥] Zhenhua Zhang,[#] Haiqing Zhou,[⊥∥] Xianming Zhang,[†] Boris I. Yakobson,[⊥§] William A. Goddard III,[¶] Xia Guo,[‡*] Robert H. Hauge[⊥∥1] and James M. Tour[⊥∥§*]

[†]Institute of Crystalline Materials, Shanxi University, Taiyuan, Shanxi 030006, China

[‡]College of Electronic Information and Control Engineering, [#]Institute of Microstructures and Properties of Advanced Materials, Beijing University of Technology, Beijing 100124, China

[⊥]Department of Chemistry, [∥]NanoCarbon Center, [§]Department of Materials Science and NanoEngineering, Rice University, Houston, Texas 77005, United States

[¶]Materials and Process Simulation Center, [ς]The Resnick Sustainability Institute, California Institute of Technology, Pasadena, CA 91125, USA

E-mail: tour@rice.edu, guo@bjut.edu.cn, fxiujun@gmail.com

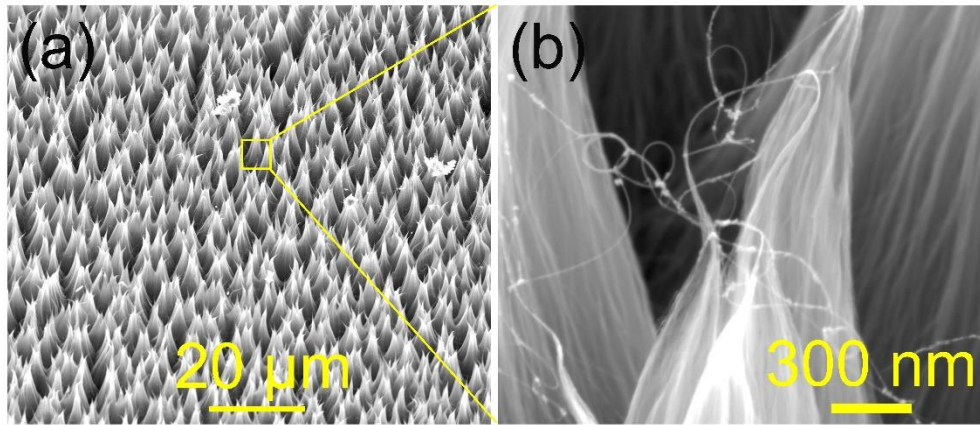[1] Deceased March 17, 2016

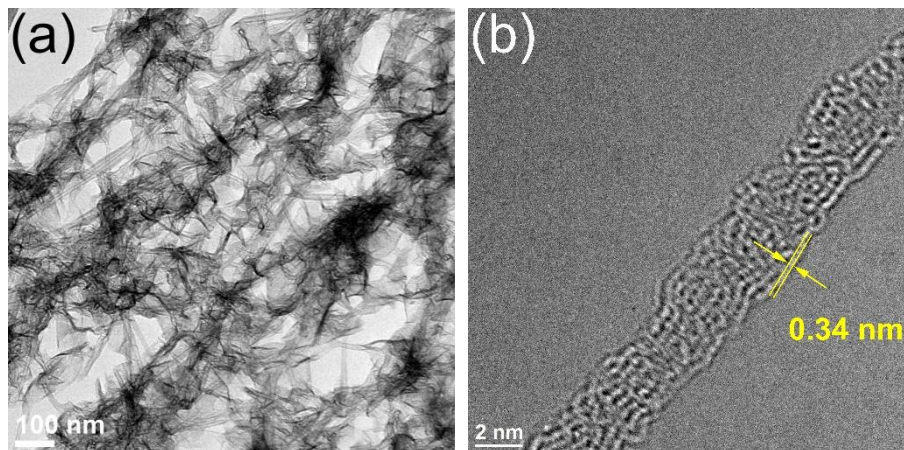**Figure S1.** SEM images of VA-GNR.

Figure S2. TEM images of VA-GNR showing that with atomic hydrogen treatment, VA-CNTs were unzipped and transformed into VA-GNR.
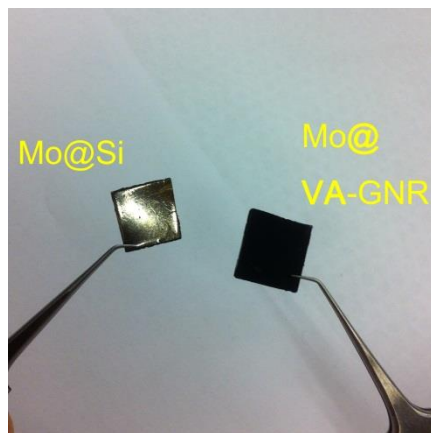
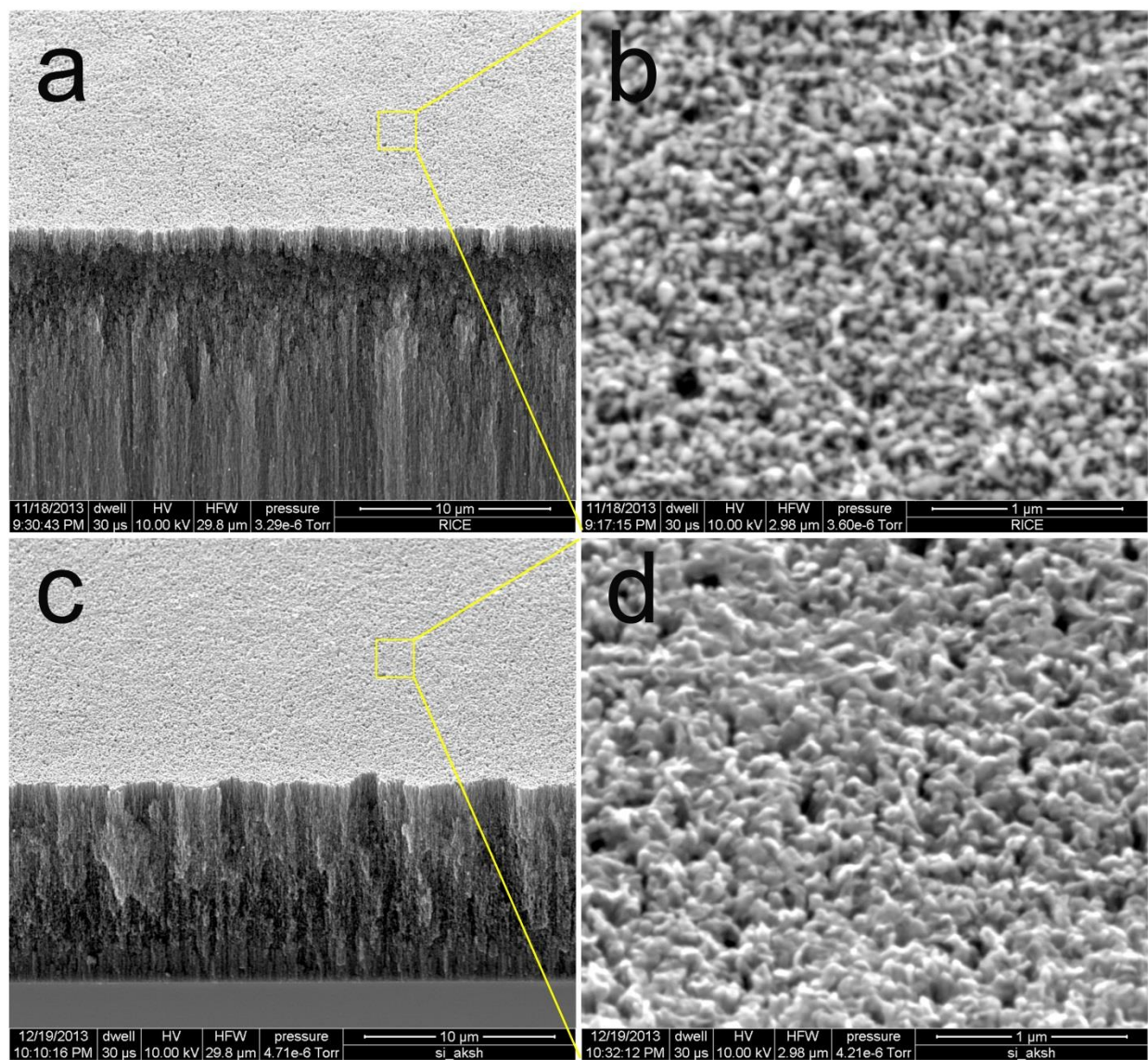**Figure S3.** Photograph of Mo@Si (left) and Mo@VA-GNR (right).

Figure S4. SEM images of Mo$_2$C-GNR hybrid grown with various growth time (a,b) for 3 h and (c,d) for 9 h.
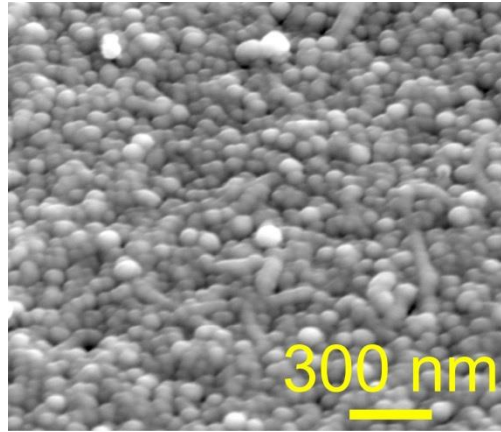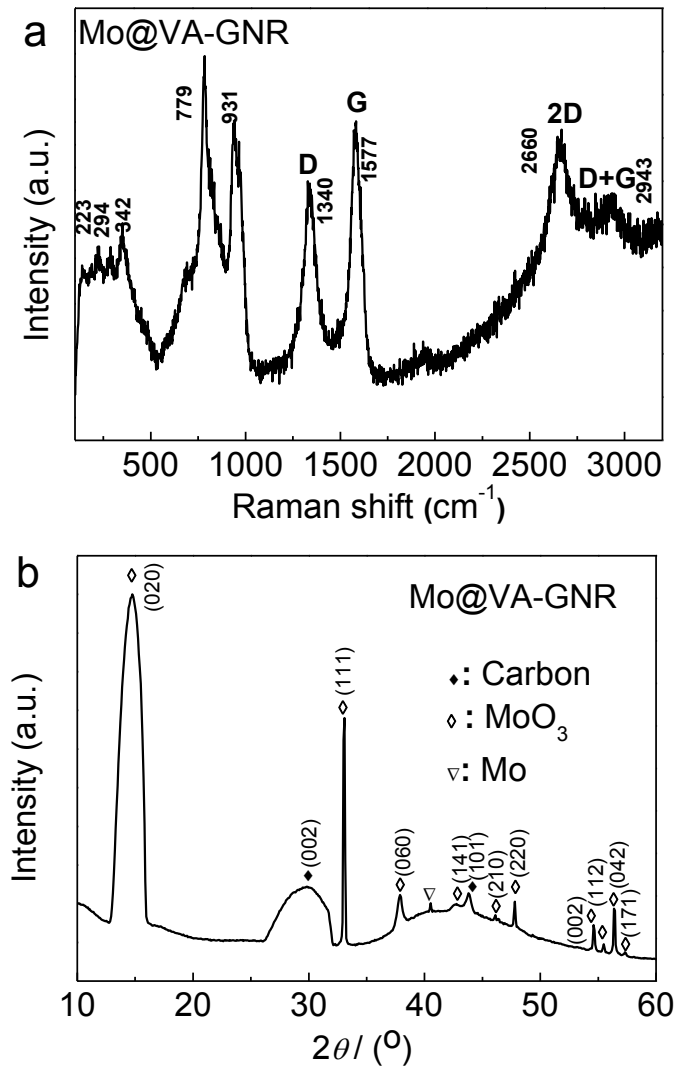
Figure S5. SEM image of Mo$_2$C on Si.

Figure S6. (a) Raman spectra of VA-GNR with molybdenum deposited on the top layers. Mo@VA-GNR has characteristic peaks at 223, 294, 342, 779, and 931 cm^{-1} that can be assigned to MoO$_3$. (b) XRD patterns of Mo@VA-GNR.
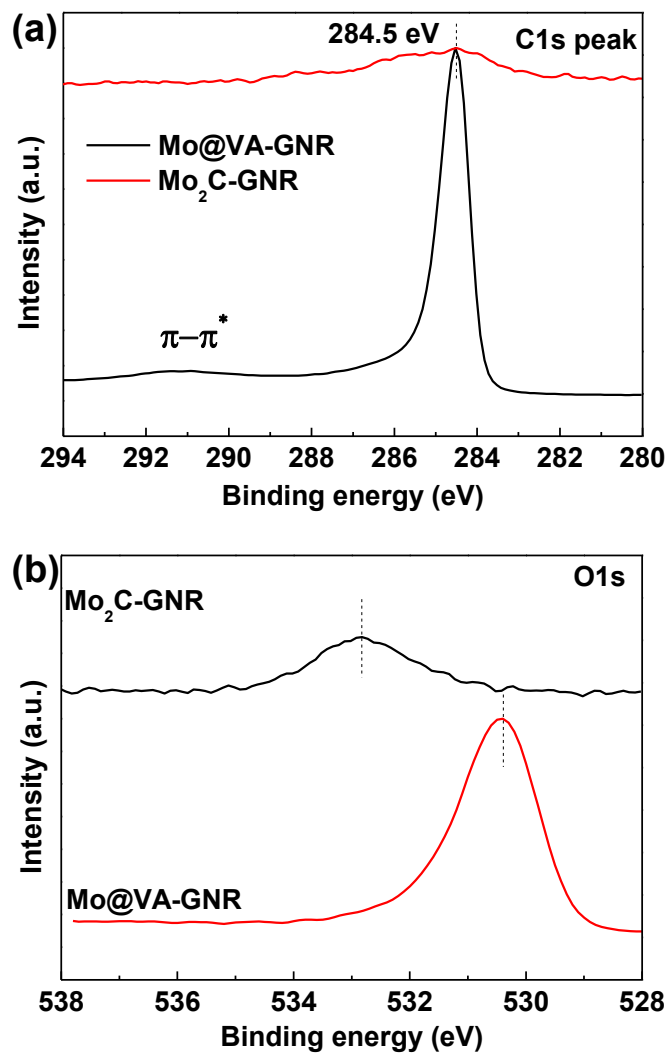
Figure S7. XPS spectrum of Mo@VA-GNR and Mo_2C-GNR hybrid for (a) C 1s and (b) O 1s.

The O 1s spectrum (b) for the Mo@VA-GNR contained a characteristic signal at 530.4 eV that is assigned to O_2^- in MoO_3.[1] For Mo_2C-GNR, the O 1s peak becomes prominent and shifts to 532.8 eV, which can be attributed to physisorbed O.
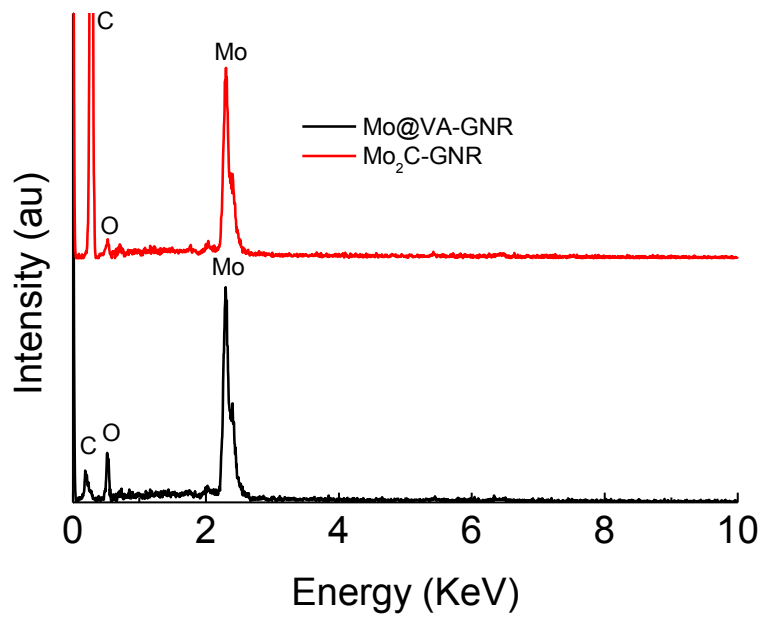
Figure S8. The results of qualitative EDS of (black curve) Mo@VA-GNR and (red curve) Mo_2C-GNR.

Table S1. Mo content determined by ICP-MS and quantitative surface analysis by EDS.

Samples	Mo loading (wt%)	Surface atomic concentration (at%)		
		C	O	Mo
Mo@VA-GNR	31.5	21.0	50.6	28.4
Mo_2C-GNR	31.3	66.3	3.5	30.2
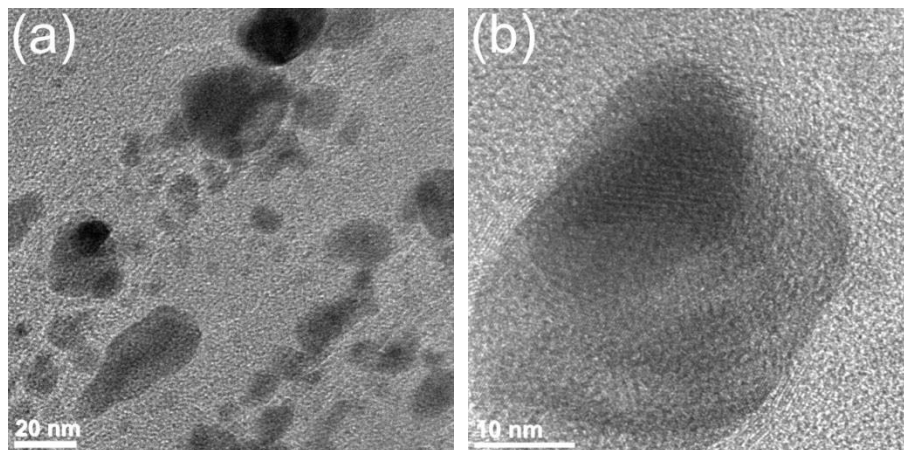
Figure S9. TEM images of Mo$_2$C.
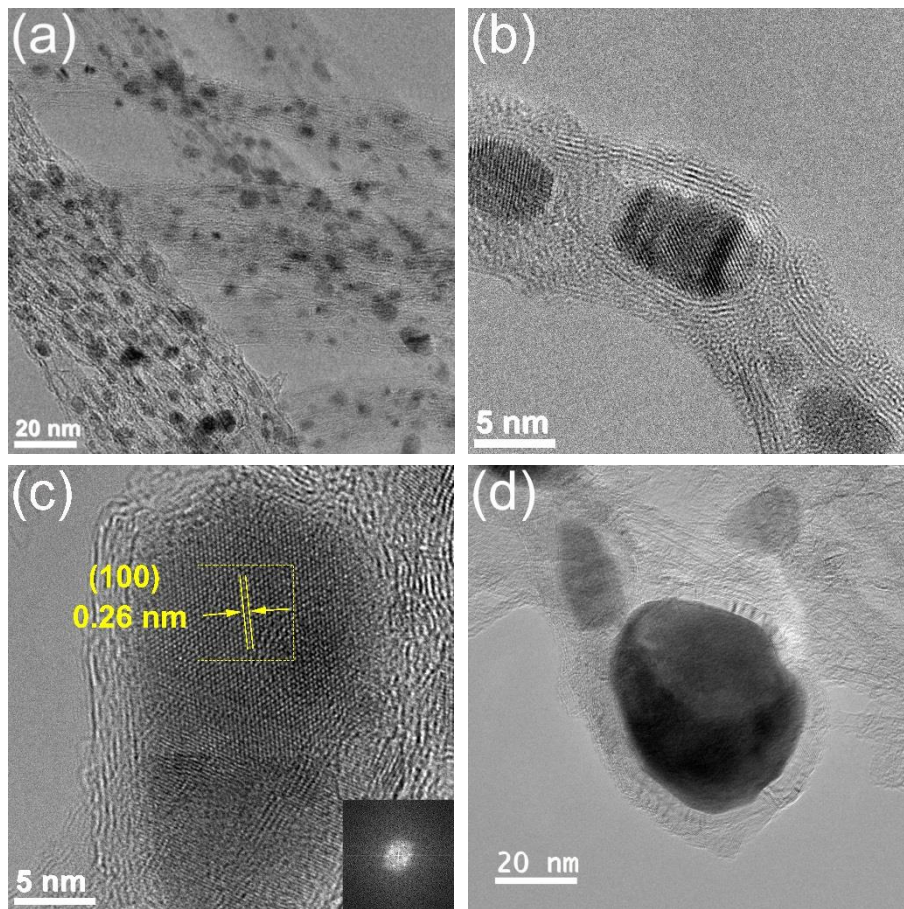
Figure S10. The TEM images of Mo$_2$C-GNR grown with various growth time, (a-b) for 3 h and (c-d) for 9 h.
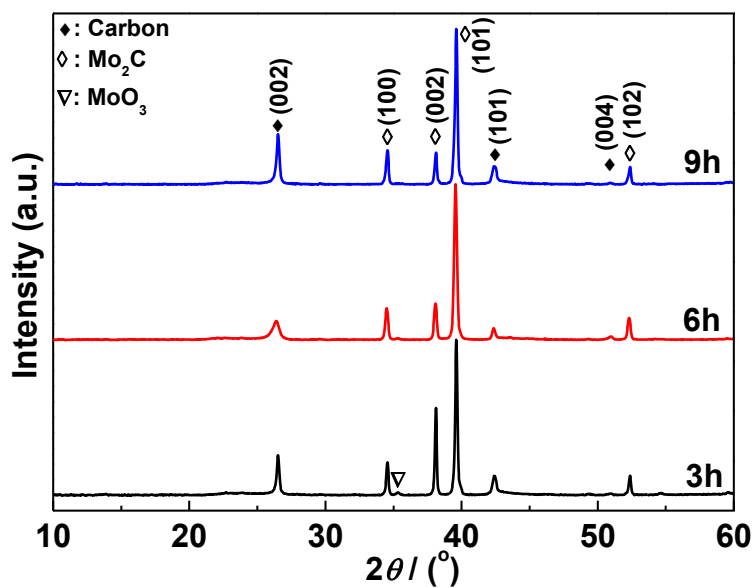
Figure S11. XRD patterns of Mo₂C-GNR grown with various growth time, from 3 to 9 h. From this data, it is confirmed that Mo₂C was successfully synthesized on GNRs in the Mo₂C-GNR hybrid.
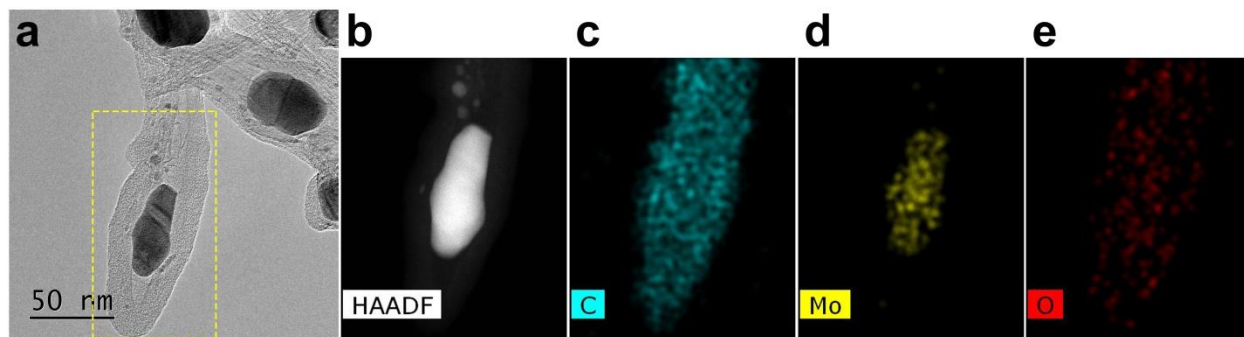
Figure S12. (a) TEM, (b) HAADF image of Mo_2C-GNR prepared with atomic H treatment for 9 h and element maps of (c) C, (d) Mo, and (e) O.
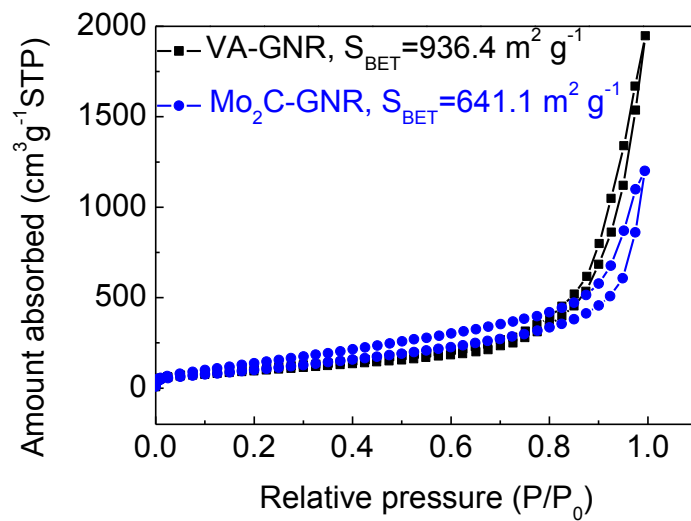
Figure S13. Nitrogen sorption isotherms of VA-GNR and Mo$_2$C-GNR hybrid.
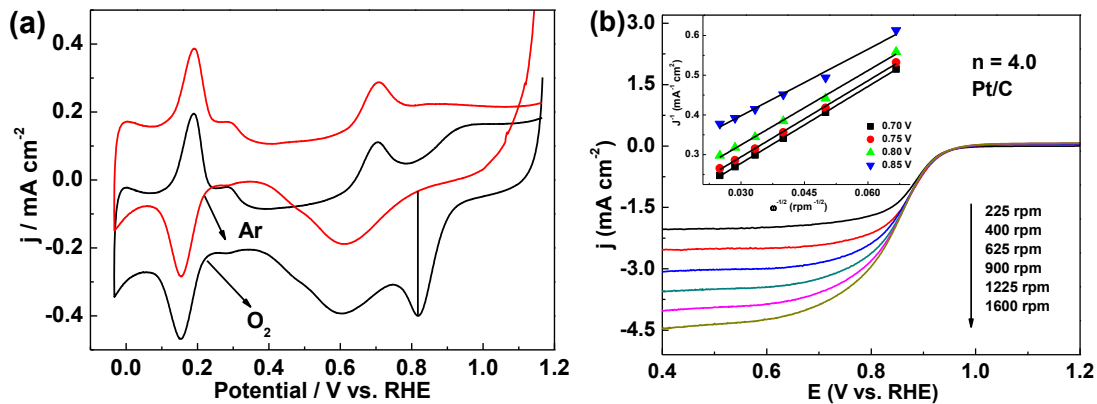
Figure S14. (a) CV of Pt/C in Ar- (red) and O_2- (black) saturated electrolyte. (b) LSVs of Pt/C in O_2-saturated 0.1 M KOH at a scan rate of 5 mV s^{-1} at different RDE rotation rates (in rpm). Inset reveals corresponding Koutecky-Levich plots (J^{-1} *vs* rpm $^{-1-2}$) at different potentials.
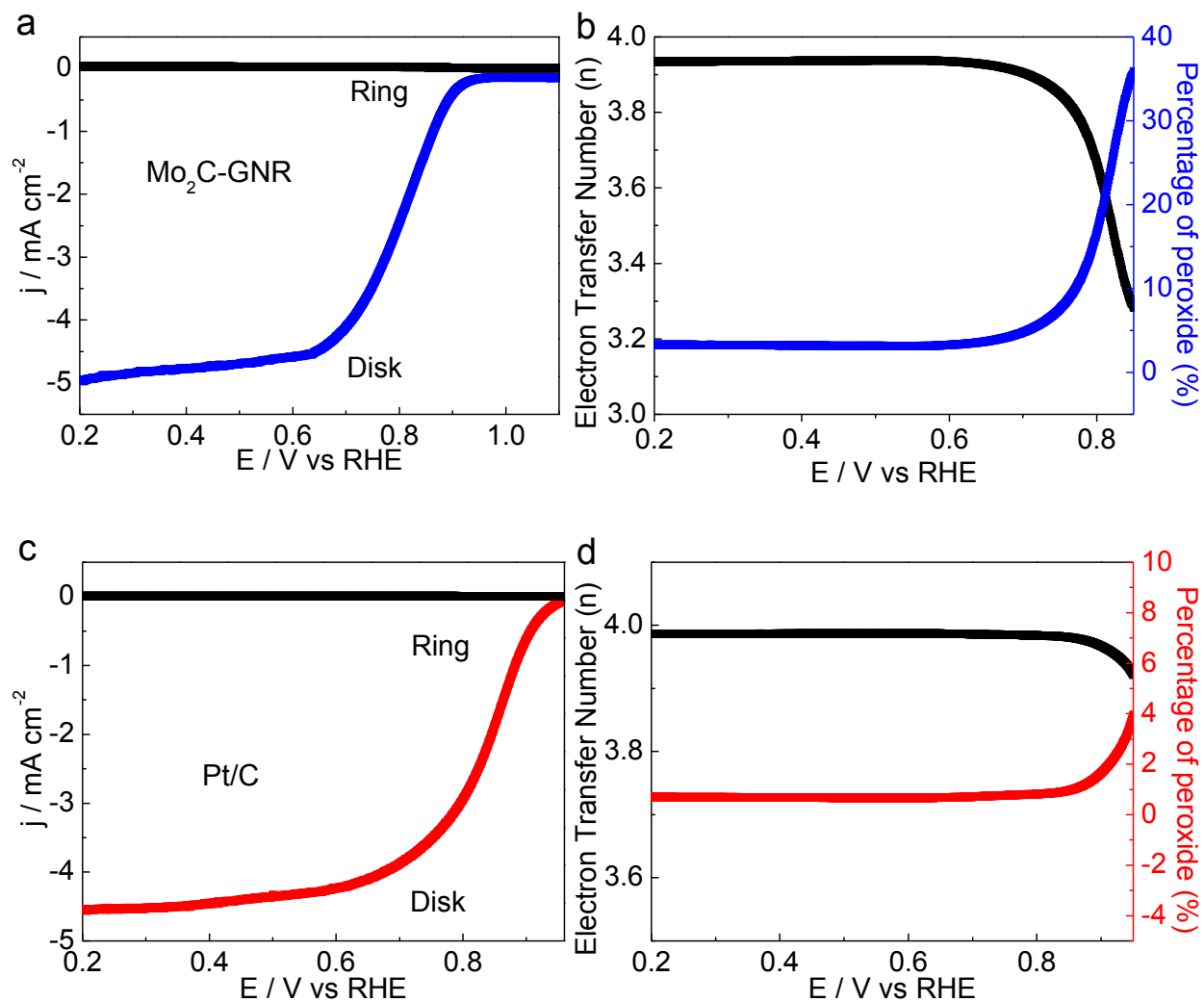
Figure S15. (a,c) Rotating ring disk electrode (RRDE) voltammograms of ORR on Mo_2C-GNR and Pt/C electrode, respectively, with a sweep rate of 5 mv s^{-1} at 1600 rpm. (b,d) Percentage of peroxide and the electron transfer number (n) of Mo_2C-GNR and Pt/C at different potentials derived from the RRDE data.
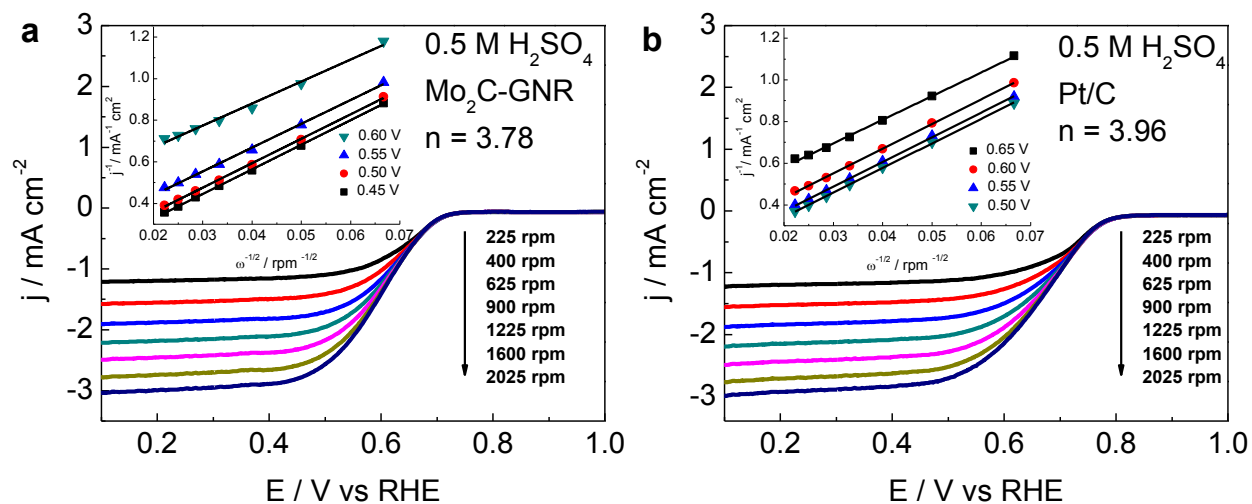
Figure S16. LSVs at 5 mV s^{-1} in the presence of oxygen with rotation speed from 225 to 2025 rpm in 0.5 M H$_2$SO$_4$ for (a) Mo$_2$C-GNR grown with 6 h and (b) Pt/C. The insets in each panel are the corresponding Koutecky-Levich plots (J^{-1} *vs* rpm $^{-1/2}$) at different potentials.
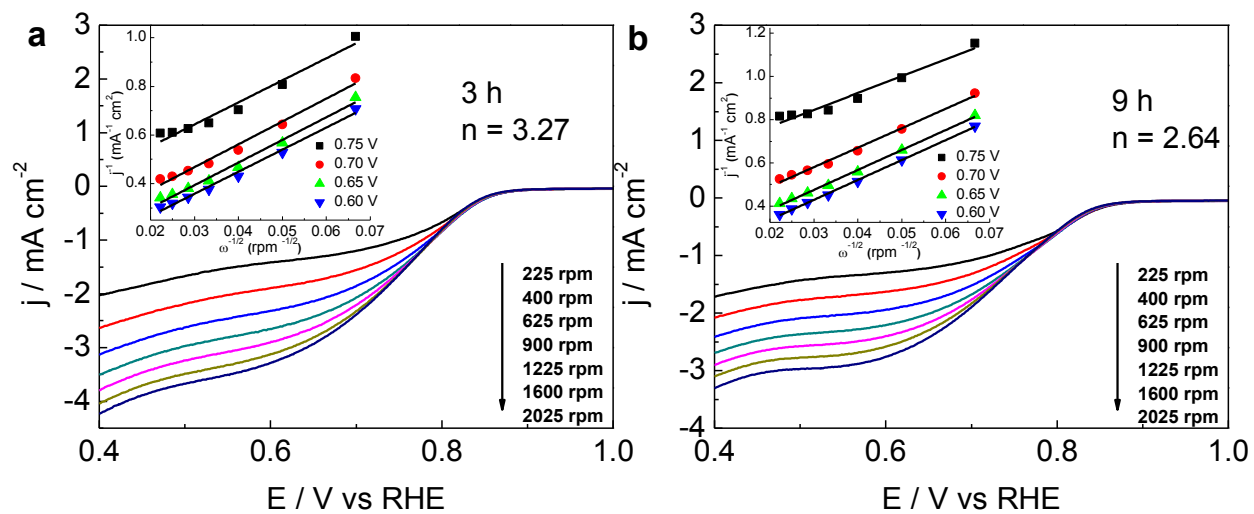
Figure S17. Rotating-disk voltammograms of Mo₂C-GNR grown with various time in O₂-saturated 0.1 M KOH at a scan rate of 5 mV s⁻¹ at different rotating speeds, (a) 3 h and (b) 9 h. Insets are the corresponding Koutecky-Levich plots at different potentials.

ORR Activity Calculations

The working electrode was scanned cathodically at a rate of 5 mV s^{-1} with varying rotating speed from 225 to 2025 rpm. Koutecky–Levich plots (J^{-1} *vs* $\omega^{-1/2}$) were analyzed at various electrode potentials. The slopes of their best linear fit lines were used to calculate the number of electrons transferred (n) on the basis of the Koutecky–Levich eq 1-3:

$$\frac{1}{J} = \frac{1}{J_K} + \frac{1}{J_L} = \frac{1}{J_K} + \frac{1}{B\omega^{1/2}} \quad (1)$$

$$B = 0.62nFC_0D_0^{2/3}\gamma^{1/6} \quad (2)$$

$$J_K = nFKC_0 \quad (3)$$

where J is the measured current density, J_k and J_L are the kinetic- and diffusion-limiting current densities, ω is the angular velocity, n is transferred electron number, F is the Faraday constant (96 485 C mol^{-1}), C_0 is the bulk concentration of O$_2$ (1.2×10^{-6} mol cm^{-3}), and v is the kinetic viscosity of the electrolyte (0.01 cm^2 s^{-1} for both 0.5 M H$_2$SO$_4$ solution and 0.1 M KOH solution), D_0 is the O$_2$ diffusion coefficient (1.9×10^{-5} cm^2 s^{-1}), and k is the electron-transfer rate constant. The number of electrons transferred (n) and J_k can be obtained from the slope and intercept of the Koutecky–Levich plots, respectively.

For the RRDE measurements, catalyst inks and electrodes were prepared by the same method as those of RDE. The disk electrode was scanned at a rate of 5 mV s^{-1} and the ring potential was kept constant at 0.5 V vs. Ag/AgCl. The H$_2$O$_2$ eq 4 and 5

$$H_2O_2 \text{ (\%)} = 100 \times \frac{2I_r/N}{I_d + I_r/N} \quad (4)$$

$$n = 4 \times \frac{I_d}{I_d + I_r/N} \quad (5)$$

Here, I_d is disk current, I_r is ring current and $N = 0.36$ is collection efficiency (N).
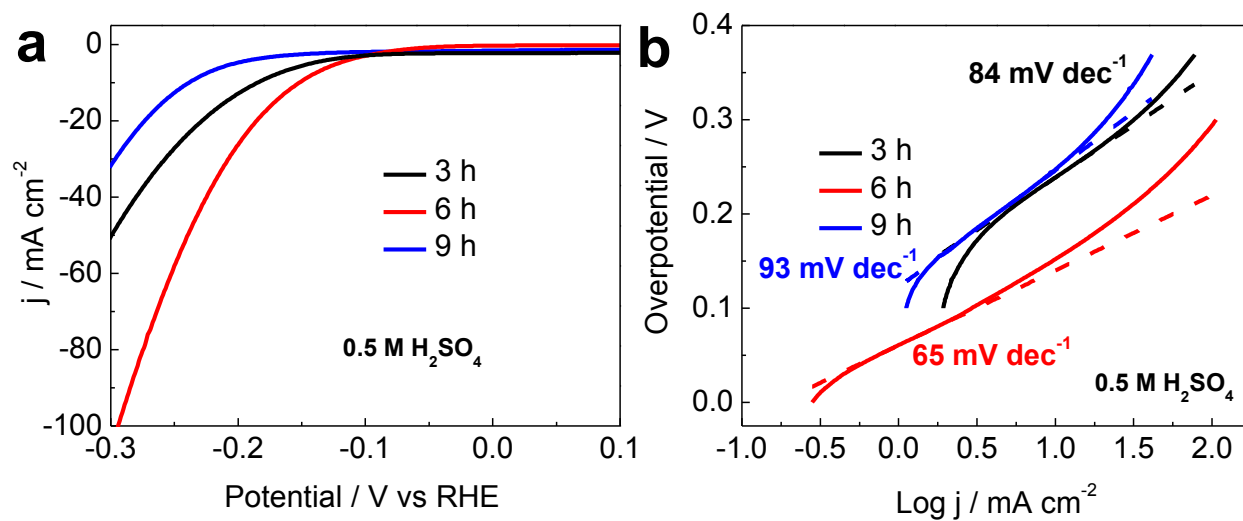
Figure S18. (a) HER polarization curves and (b) the corresponding Tafel plots of Mo_2C-GNR grown with various growth time.
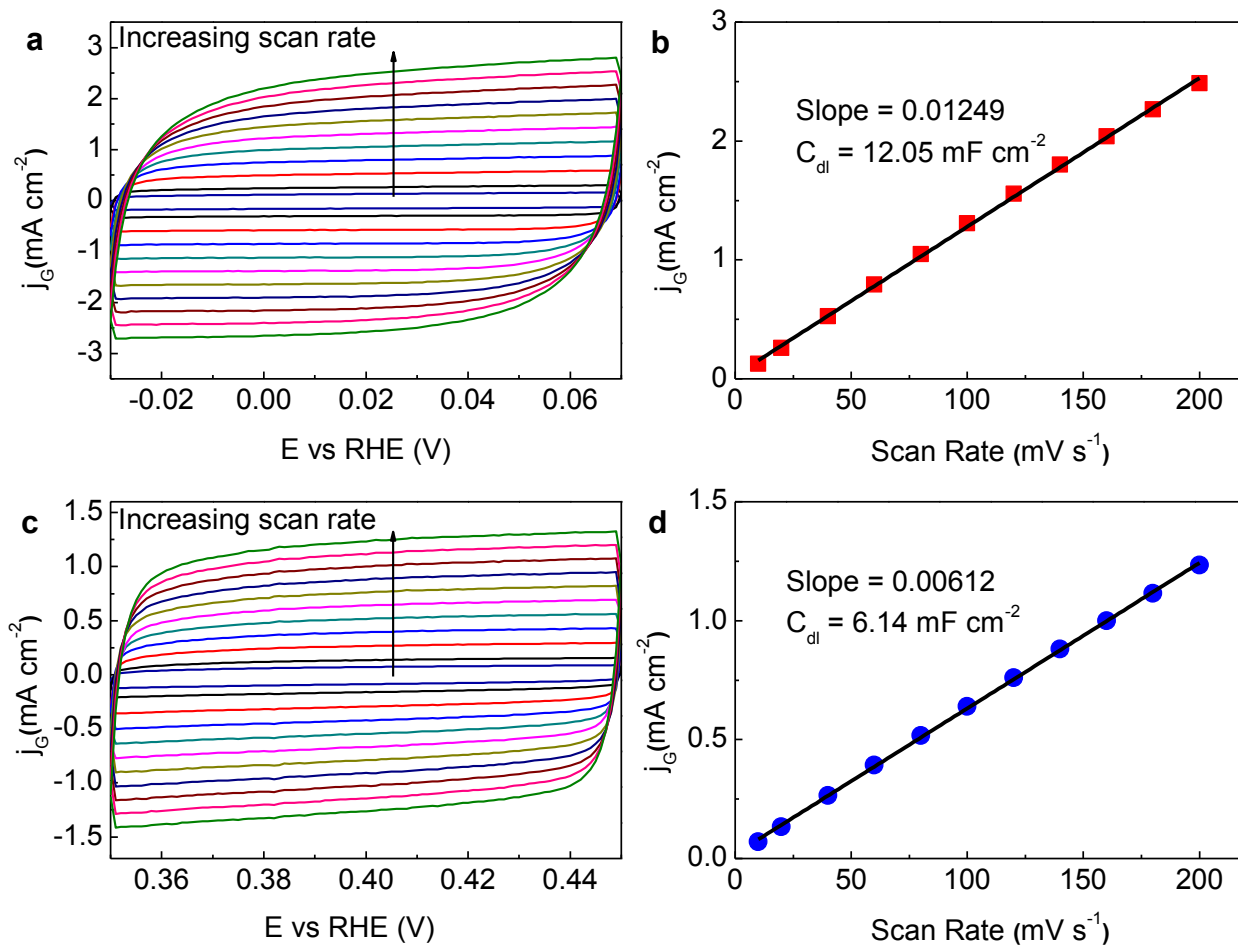
Figure S19. Cyclic voltammograms and capacitive currents plotted as a function of scan rate in 0.5 M H_2SO_4 at scan rates of 10, 20, 40, 60, 80, 100, 120, 140, 160, 180 and 200 mV s^{-1} for Mo_2C-GNR grown with various time, (a,b) 3 h and (c,d) 9 h.

The effective surface areas of Mo_2C-GNR grown at various times were compared by estimating their electrochemical double layer capacitances (C_{dl}) with cyclic voltammograms (CVs). CVs were performed at a potential range of (-0.03) to 0.07 V *vs* RHE and 0.35 to 0.45 V *vs* RHE, respectively, where no obvious electrochemical features corresponding to the Faradic current were observed (Figure S19 a and c). The capacitive currents, $\Delta j(j_a$-$j_c)$@0.02 V and

$\Delta j(j_a-j_c)$@0.40 V, were plotted against the scan rate (Figure S19 b and d). The linear relationships were observed with the slopes twice the C_{dl} value. Accordingly, the C_{dl} values for Mo$_2$C-GNR grown with 3 h and 9 h were calculated to be 12.05 and 6.14 mF cm^{-2}, respectively.
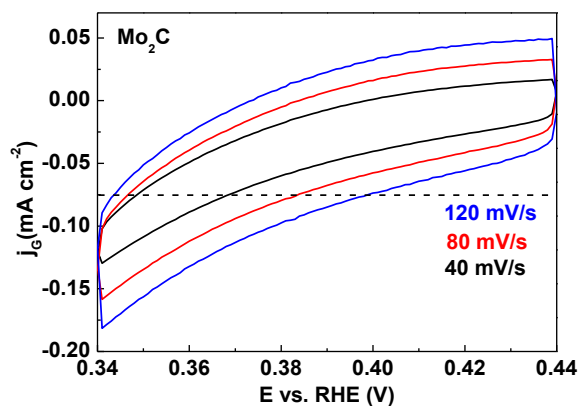
Figure S20. CV curves of Mo$_2$C in acidic medium.

HER Activity Calculations

The electrochemically active surface area (EASA) was estimated from the electrochemical double-layer capacitance of the nanoporous layers. The double layer capacitance (C_{dl}) was determined with a simple cyclic volatammetry (CV) method. The EASA is then calculated from the double-layer capacitance according to eq 6:

$$\text{EASA} = \frac{C_{dl}}{C_s} \quad (6)$$

Where C_s is the capacitance of an atomically smooth planar surface of the material per unit area under identical electrolyte conditions. An average value of $C_s = 22\ \mu\text{F cm}^{-2}$ is used in this work. The roughness factor (RF) is then calculated by dividing the estimated EASA by the geometric area of the electrode.
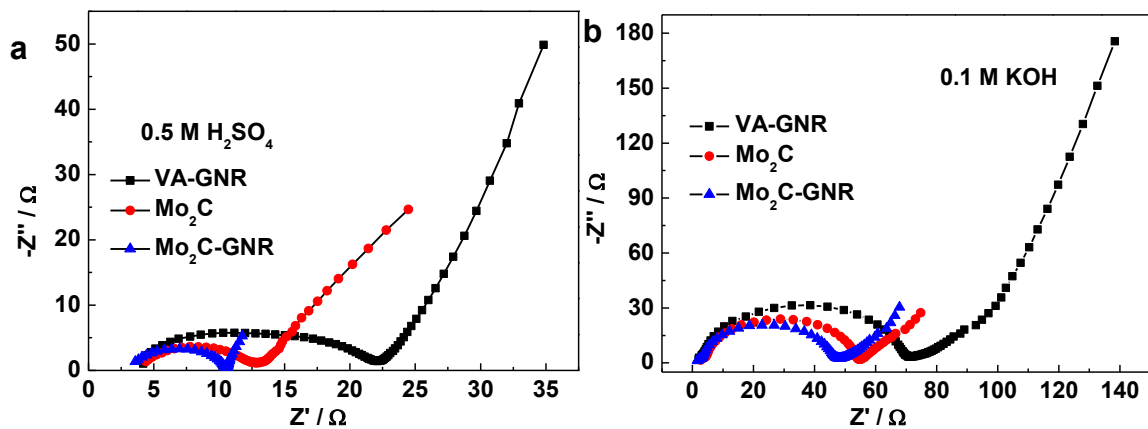
Figure S21. Nyquist plots with an equivalent circuit in (a) acidic and (b) alkaline medium.
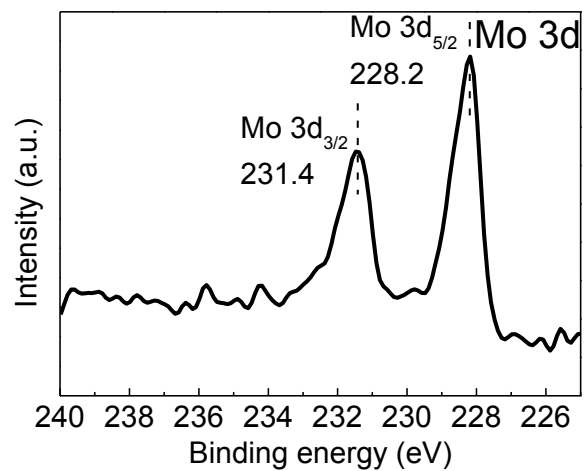
Figure S22. Mo 3d XPS spectrum of Mo$_2$C-GNR after a 30000 s durability test.

Table S2. ORR electrochemical analysis of Mo_2C, Mo_2C-GNR, VA-GNR and Pt/C catalyst.

Catalysts	Surface area [a] m² g⁻¹	Sheet resistance [b] Ω □⁻¹	E_{peak} V	j_{peak} mA cm⁻²	E_{onset} V	Half-wave potential [c] V	j [d] mA cm⁻²
Mo_2C	28	456	0.73	0.09	0.84	0.71	2.76
Mo_2C-GNR	641.1	76.8	0.83	2.01	0.93	0.81	4.55
VA-GNR	936.4	1065.2	0.68	0.41	0.82	0.73	1.43
Pt/C	-	-	0.82	0.41	0.96	0.84	4.40

[a]From BET method. [b]From 4-point probe method. [c]The half-wave potential represents the potential at which the current is half of the limiting current in the LSV curve. [d]Measured at 0.5 V *vs* RHE, 1600 rpm.

Table S3. HER electrochemical properties of Mo_2C, Mo_2C-GNR, and Pt catalysts.

Catalyst		η @ 10 mA cm^{-2} mV	Onset potential mV	J @ 300 mV mA cm^{-2}	Tafel slope mV dec^{-1}	R_{ct}[a] Ω
Mo_2C	0.5 M H$_2$SO$_4$	275	106	14.1	129	12.9
	0.1 KOH	266	124	14.6	147	68.9
Mo_2C-GNR	0.5 M H$_2$SO$_4$	152	39	106.2	69	10.5
	0.1 KOH	121	53	31.2	59	47.8
Pt	0.5 M H$_2$SO$_4$	26.5	5	6030	30	-
	0.1 KOH	15	6	1510	29	-

[a]Extracted from fitting electrochemical impedance spectra measured at η = 5 mV to an equivalent circuit.

Table S4. Comparison of HER activity of some Mo-based catalysts.

Catalysts	Electrolyte	Tafel slope mV dec^{-1}	Onset overpotential mV	Metal precursor	ref
Mo$_2$C-GNR	**0.5 M H$_2$SO$_4$**	**65**	**39**	**Mo**	**This work**
Mo$_2$C-GNR	**0.1 M KOH**	**59**	**53**	**Mo**	**This work**
Mo$_2$C/GCSc	0.5 M H$_2$SO$_4$	62.6	120	(NH$_4$)$_6$Mo$_7$O$_{24}$·4H$_2$O	2
Mo$_2$C/CNTs	0.1 M HClO$_4$	55.2	63	(NH$_4$)$_6$Mo$_7$O$_{24}$·4H$_2$O	3
Mo$_2$C/XC	0.1 M HClO$_4$	59.4	105	(NH$_4$)$_6$Mo$_7$O$_{24}$·4H$_2$O	3
Mo$_2$C/CNTs-GR	0.5 M H$_2$SO$_4$	58	62	MoCl$_5$	4
Mo$_2$C-RGO	0.5 M H$_2$SO$_4$	54	~70	(NH$_4$)$_6$Mo$_7$O$_{24}$·4H$_2$O	5
Mo$_2$C-NWs	0.5 M H$_2$SO$_4$	55.8	~160	(NH$_4$)$_6$Mo$_7$O$_{24}$·4H$_2$O	6
Mo$_2$C-NSs	0.5 M	64.5	~160	(NH$_4$)$_6$Mo$_7$O$_{24}$·4H$_2$O	6

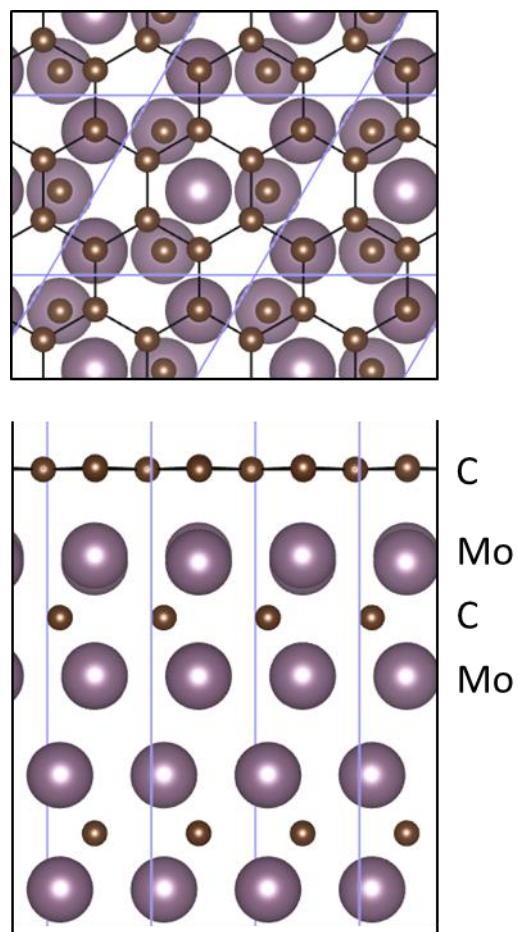| Catalysts	Electrolyte	Tafel slope mV dec^{-1}	Onset overpotential mV	Metal precursor	ref
Np-Mo$_2$C NWs	H$_2$SO$_4$ 0.5 M H$_2$SO$_4$	54	~70	(NH$_4$)$_6$Mo$_7$O$_{24}$·4H$_2$O	7
Mo$_2$C-NCNTs	0. 5 M H$_2$SO$_4$	71	72	MoO$_3$	8
MoS$_2$/Mo$_2$C-NCNTs	0. 5 M H$_2$SO$_4$	69	145	MoO$_3$	9

Figure S23. Structure model for Mo_2C-graphene hybrid. The blue lines show the boundaries of the periodic cell.

References

1. Hanawa, T.; Hiromoto, S.; Asami, K. Characterization of the Surface Oxide Film of a Co–Cr–Mo Alloy After Being Located in Quasi-Biological Environments Using XPS. *Appl. Surf. Sci.* **2001**, *183*, 68-75.

2. Cui, W.; Cheng, N.; Liu, Q.; Ge, C.; Asiri, A. M.; Sun, X. Mo_2C Nanoparticles Decorated Graphitic Carbon Sheets: Biopolymer-Derived Solid-State Synthesis and Application as an Efficient Electrocatalyst for Hydrogen Generation. *ACS Catal.* **2014**, *4*, 2658-2661.

3. Chen, W. F.; Wang, C. H.; Sasaki, K.; Marinkovic, N.; Xu, W.; Muckerman, J. T.; Zhu, Y.; Adzic, R. R. Highly Active and Durable Nanostructured Molybdenum Carbide Electrocatalysts for Hydrogen Production. *Energy Environ. Sci.* **2013**, *6*, 943-951.

4. Youn, D. H.; Han, S.; Kim, J. Y.; Kim, J. Y.; Park, H.; Choi, S. H.; Lee, J. S. Highly Active and Stable Hydrogen Evolution Electrocatalysts Based on Molybdenum Compounds on Carbon Nanotube–Graphene Hybrid Support. *ACS Nano* **2014**, *8*, 5164-5173.

5. Pan, L. F.; Li, Y. H.; Yang, S.; Liu, P. F.; Yu, M. Q.; Yang, H. G. Molybdenum Carbide Stabilized on Graphene with High Electrocatalytic Activity for Hydrogen Evolution Reaction. *Chem. Commun.* **2014**, *50*, 13135-13137.

6. Ge, C.; Jiang, P.; Cui, W.; Pu, Z.; Xing, Z.; Asiri, A. M.; Obaid, A. Y.; Sun, X.; Tian, J. Shape-Controllable Synthesis of Mo_2C Nanostructures as Hydrogen Evolution Reaction Electrocatalysts with High Activity. *Electrochim. Acta* **2014**, *134*, 182-186.

7. Liao, L.; Wang, S.; Xiao, J.; Bian, X.; Zhang, Y.; Scanlon, M. D.; Hu, X.; Tang, Y.; Liu, B.;

Girault, H. H. A Nanoporous Molybdenum Carbide Nanowire as an Electrocatalyst for Hydrogen Evolution Reaction. *Energy Environ. Sci.* **2014**, *7*, 387-392.

8. Zhang, K.; Zhao, Y.; Fu, D.; Chen, Y. Molybdenum Carbide Nanocrystal Embedded N-Doped Carbon Nanotubes as Electrocatalysts for Hydrogen Generation. *J. Mater. Chem. A* **2015**, *3*, 5783-5788.

9. Zhang, K.; Zhao, Y.; Zhang, S.; Yu, H.; Chen, Y.; Gao, P.; Zhu, C. MoS_2 Nanosheet/Mo_2C-Embedded N-Doped Carbon Nanotubes: Synthesis and Electrocatalytic Hydrogen Evolution Performance. *J. Mater. Chem. A* **2014**, *2*, 18715-18719.